AIAA JOURNAL
Vol. 59, No. 5, May 2021

Links Between Steepened Mach Waves and Coherent Structures for a Supersonic Jet

Pierre Pineau* and Christophe Bogey†
Laboratoire de Mécanique des Fluides et d'Acoustique, UMR 5509, F-69134 Ecully, France

https://doi.org/10.2514/1.J059859

The links between coherent structures in the shear layer of an isothermal Mach 2 jet and steepened Mach waves just outside the jet are investigated using large-eddy simulation. Conditional averages triggered by the detection of high-intensity pressure peaks on a conical surface near the jet flow are computed. Averages obtained for peaks of different intensities are presented to identify the factors favoring the steepened aspect of the waves, which are not likely due to nonlinear propagation effects given the surface radial position. The Mach waves just outside the jet are shown to be correlated with coherent structures in the supersonic side of the mixing layers. Their steepened aspect is found to increase with their intensity. The variations of the wave properties with the convection speed, strength, and geometrical shape of the mixing layer structures are then discussed. These properties do not depend much on the convection speed but are closely related to the two other parameters. The wave intensity and steepened aspect increase because the shear-layer structures are stronger, but also because they are more inclined relative to the jet direction. In the latter case, the asymmetric shape of the structure appears to promote the formation of positively skewed Mach waves.

Downloaded by ECOLE CENTRAL DE LYON on May 8, 2021 | http://arc.aiaa.org | DOI: 10.2514/1.J059859

Nomenclature

a	=	speed of sound
D	=	jet diameter
M	=	Mach number
p	=	pressure
Re_D	=	diameter-based Reynolds number
r	=	radial coordinate
r_s	=	specific ideal gas constant
r_0	=	jet radius
T	=	temperature
t	=	time
u	=	velocity
z	=	axial coordinate
Δr	=	radial mesh spacing
Δz	=	axial mesh spacing
$\Delta\theta$	=	azimuthal resolution
θ	=	azimuthal coordinate
α	=	Mach wave radiation angle
γ	=	ratio of specific heats
ν	=	kinematic viscosity
ρ	=	density
τ	=	interval length for the conditional averages

Subscripts

j	=	initial value of the jet parameters
s	=	stagnation quantity
trig	=	conditional averages trigger
∞	=	ambient quantity

Superscript

$'$	=	fluctuating quantity

Received 15 June 2020; revision received 24 October 2020; accepted for publication 9 November 2020; published online 31 December 2021. Copyright © 2020 by the authors. Published by the American Institute of Aeronautics and Astronautics, Inc., with permission. All requests for copying and permission to reprint should be submitted to CCC at www.copyright.com; employ the eISSN 1533-385X to initiate your request. See also AIAA Rights and Permissions www.aiaa.org/randp.

*Postdoctoral Fellow; also University of Lyon, Ecole Centrale de Lyon, INSA Lyon, Université Claude Bernard Lyon I, CNRS; pierre.pineau@ec-lyon.fr.

†CNRS Research Scientist; also University of Lyon, Ecole Centrale de Lyon, INSA Lyon, Université Claude Bernard Lyon I, CNRS. Senior Member AIAA.

I. Introduction

HIGH-SPEED supersonic jets such as those exiting from the jet engines powering modern military aircrafts produce a distinctive, particularly unpleasant sound known as crackle [1], which has been related to the presence of steep, jagged shock structures in their acoustic fields. These steepened waves primarily occur in the downstream direction, where acoustic levels are strongest, and have been reported near jets issued from model-scale nozzles [2–5] as well as full-scale engines [1,6,7]. Several nonlinear mechanisms are involved in the formation of these waves. Notably, nonlinear propagation effects due to high-pressure levels in the acoustic field can cause a gradual steepening of the waves as they propagate away from the flow, leading to the formation of shocks as observed, for instance, by Gee et al. [7] for full-scale jet engines. Another consequence of nonlinear propagation effects is the coalescence of neighboring waves, which leads to fewer and stronger shocks as the propagation distance increases [8,9]. As argued by Lighthill [10], this mechanism promotes the formation of extreme, intermittent, steepened waves such as those responsible for the perception of crackle. For a given broadband signal, the propagation distance required for shock formation can be estimated based on the initial wave amplitude and peak frequency [11]. Based on the model of Baars et al. [12] for spherically spreading waves, this distance ranges from just a few diameters for full-scale jet engines to several hundred for laboratory-scale tests, which is beyond the typical propagation distances considered in anechoic chambers. Moreover, for small-scale nozzles, the peak frequencies are higher than for full-scale nozzle so that the effects of molecular absorption, which counteract shock formation, are stronger. It is thus likely that nonlinear propagation effects are not the only mechanism at play in the formation of crackle. This has led some authors to argue that shock formation also occurs at the source, inside the turbulent flow, which has been confirmed by optical visualizations [5,13,14], as well as numerical simulations [15–17] of jets and mixing layers showing the presence of shocklets embedded inside the turbulent flow and propagating in the far field.

Despite several years of research, this source steepening mechanism is still not fully understood. For highly supersonic jets, the dominant noise component in the downstream direction, where crackle perception is most intense, consists of Mach waves generated by coherent structures [18,19]. These structures are convected at a supersonic speed u_c inside the jet flow and lead to a peak of noise emission for an angle α given by

$$\cos\alpha = \frac{a_\infty}{u_c} \tag{1}$$

with respect to the jet direction, where a_∞ is the speed of sound in the ambient medium. Since coherent structures act upon the ambient medium as wavy walls or bluff bodies, the formation of shocks is not surprising as soon as the convection velocity exceeds the speed of sound. However, in most models of Mach wave radiation, coherent structures and their associated pressure fields are modeled as linear instability waves [20–23]. These models correctly predict several important features of Mach wave radiation, such as the direction of maximum noise level or the shape of the spectra near the peak frequency, but fail to take into account the possible presence of shocks, due to their linear nature. Therefore, further investigations are required in order to characterize the formation mechanism of steepened Mach waves, and to highlight what particular aspects of the source (that is, the coherent structures) cause the wave fronts to steepen near the jet. This is particularly important since previous studies have shown that modifying these structures using noise reduction devices such as chevrons [24], microjets [25], or nozzle inserts [26] could reduce the crackling behavior of supersonic jets.

Recently, by combining simulations of temporally developing plane mixing layers and a parametric analysis of supersonic flows over wavy surfaces, Buchta and Freund [16,27] related the skewness of the near-pressure field, and hence its nonlinearity, to the convection speed and the magnitude of the turbulent fluctuations. Similar results were obtained by the authors of the present paper using numerical simulations of temporally developing axisymmetric mixing layers [28–30]. In the latter studies, the coherent structures generating the steepened waves were extracted by averaging a large number of flow events correlated with intense pressure peaks near the jet flow. The shape and convection speed of the structures were both found to influence the intensity and the nonlinearity of the waves they generate. It is noteworthy that the results obtained in the aforementioned studies are based on the analysis of temporally developing model flows. These models are useful for performing parametric studies revealing the noise generation mechanisms at play. However, since they remain parallel as they grow, they differ from the spatially developing jets considered in experiments that spread with increasing distance from the nozzle. For that reason, coherent structures in spatially developing jets are expected to have different geometrical properties [31] and convection speeds [32] than those in temporally developing ones so that it is legitimate to wonder how this would affect the steepened Mach waves they generate.

In the present study, a conditional-averaging procedure very similar to the one described in Refs. [28–30,33] for temporally developing jets is applied to a numerical simulation of an isothermal Mach 2 jet in order to investigate the role of large-scale coherent structures in the steepening of Mach waves immediately inside the turbulent flow. The conditional-averaging procedure is based on the detection and synchronization of extreme pressure peaks on a conical surface spreading with the jet. This surface is located as close as possible to the jet shear layer to minimize the wave steepening due to nonlinear propagation effects. By sorting the detected peaks according to their peak intensity, the structures generating the strongest waves can be compared with those that produce the weakest ones in order to identify which of their properties favor the steepening of Mach waves. More particularly, based on previous investigations [26–28,34], the roles of the structure convection speeds, strengths, and geometrical shapes will be explored. Unlike the temporally developing flows considered in Refs. [28–30], the present jet exhausts from a nozzle and spreads with the axial coordinate so that the structure tendency to generate steepened Mach waves is expected to evolve with the distance from the nozzle. For that reason, the conditional-averaging procedure will be performed for different axial positions spanning the entire axial extent of the shear layer.

The paper is organized as follows. First, the simulation parameters and computational methods are introduced in Sec. II. Then, the conditional-averaging procedure is presented and applied to the numerical database in Sec. III. Finally, concluding remarks are given in Sec. IV.

II. Simulation parameters

A. Jet Parameters

The jet considered in the present study is isothermal and exhausts from a round straight-pipe nozzle at a static pressure p_j matching the ambient pressure of $p_\infty = 10^5$ Pa. It has an exit Mach number $M_j = u_j/\sqrt{\gamma r_s T_j}$ of two, where u_j is the exit velocity, T_j is the exit static temperature equal to the ambient temperature $T_\infty = 293$ K, $\gamma = c_p/c_v = 1.4$ is the ratio of specific heat, and r_s is the specific ideal gas constant. The total temperature of the jet is equal to $T_s = 1.8T_\infty$ and the diameter-based Reynolds number is equal to $Re_D = u_j D/\nu_j = 5 \times 10^4$, where $D = 2r_0$ is the jet diameter and ν_j is the kinematic viscosity at the nozzle exit, computed from the Sutherland's law. Inside the nozzle, a Blasius-like velocity profile with a thickness of $0.076r_0$ is prescribed. This value yields a shear-layer momentum thickness of $\delta_\theta/r_0 = 2/\sqrt{Re_D} = 8.9 \times 10^{-3}$ at the nozzle exit, following an empirical law proposed by Zaman [35] for initially laminar jets. To favor the transition of the shear layers from a laminar to a turbulent state, weak random vortical disturbances are added inside the boundary layer. They are Gaussian vortex rings of random phases and amplitudes, as in previous studies of subsonic [36] and supersonic [37,38] jets. Their amplitude is tuned in order to yield maximum turbulence intensities of 3% at the nozzle exit so that the shear layers are initially in a weakly disturbed state.

B. Numerical Methodology

The computation is a well-resolved large-eddy simulation carried out by solving the filtered compressible Navier–Stokes equations in cylindrical coordinates (r, θ, z) using high-order, low-dissipation, and low-dispersion finite difference schemes. The spatial derivatives are evaluated using centered 11-point fourth-order finite differences [39], and time integration is performed using a second-order six-stage Runge–Kutta algorithm. At the end of each time step, grid-to-grid oscillations are removed by the application of a sixth-order selective filter. This filter also serves as an implicit subgrid-scale model used to dissipate subgrid-scale energy near the grid cutoff wave number [40,41]. Since the present flow is supersonic, shocks will be formed in and near the jet flow, leading to Gibbs oscillations that are damped using a shock capturing method based on a dilatation-based adaptive filtering [42]. Near the jet axis, the singularity is treated using the method of Mohseni and Colonius [43]; and derivatives in the azimuthal direction are computed using fewer points than permitted by the grid in order to reduce the time-step constraint due to the stability condition [44]. Finally, nonreflecting boundary conditions [45,46] are applied at the inflow, outflow, and radial limits of the computational domain.

C. Computational Parameters

The computational domain extends down to $60r_0$ in the axial direction, excluding the downstream sponge zone, and out to $18r_0$ in the radial direction; and it contains a total number of $n_r \times n_\theta \times n_z = 526 \times 256 \times 2294 = 309$ million points. The axial mesh spacing Δz is constant and equal to $0.025r_0$ from the nozzle exit at $z = 0$ and down to $z = 30r_0$; after which, it gradually increases and reaches $\Delta z = 0.05r_0$ at $z = 60r_0$. The radial mesh spacing Δr is equal to $0.025r_0$ on the jet axis and reaches a minimum of $\Delta r = 0.00625r_0$ at $r = r_0$ in order to capture the fine-scale turbulent structures that are formed near the nozzle. Further away from the jet flow, it increases and reaches the value of $\Delta r = 0.05r_0$ at $r = 5r_0$; after which, it remains constant, yielding a cutoff Strouhal number of five for an acoustic wave discretized by four points per wavelength. After an initial transient period, the flow and sound fields are recorded during a total time of $2000r_0/u_j$. In particular, the data are collected every $\Delta t = 0.1r_0/u_j$ on a conical surface spreading with the jet at an angle of 11 deg. The radial location of this surface, represented in Fig. 1, is between $r = r_0$ at $z = 0$ and $r = 7r_0$ at $z = 30r_0$. It is thus very close to the turbulent flow in order to study the mechanisms leading to the steepening of Mach waves inside the jet. In addition, the azimuthal Fourier coefficient of the pressure and velocity fields are computed every $\Delta t = 0.2r_0/u_j$ up to the mode 4 for $0 \le z \le 60r_0$ and

Downloaded by ECOLE CENTRAL DE LYON on May 8, 2021 | http://arc.aiaa.org | DOI: 10.2514/1.J059859

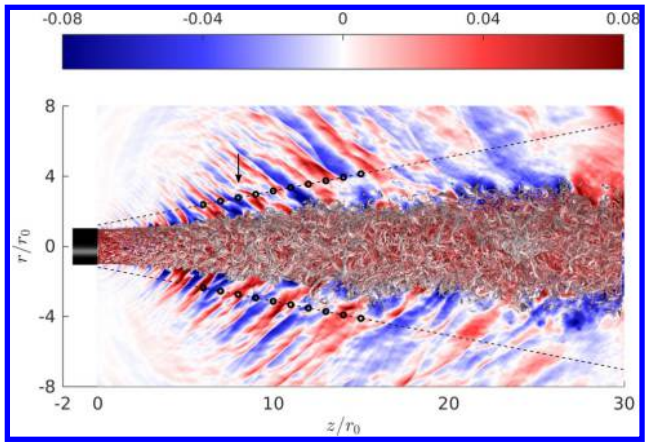

Fig. 1 Positive isosurface of q criterion $q = 0.65(u_j/r_0)^2$ colored by jet velocity and pressure fluctuations p'/p_∞ outside the jet. Circles represent detection positions for conditional averages, and the arrow indicates the location of peak pressure levels on the cylindrical surface.

$0 \leq r \leq 15r_0$. On the whole, approximately 300,000 time steps were performed, which consumed 80,000 CPU hours and generated 2 TB of data.

III. Results

A. Properties of the Near-Acoustic Field

An instantaneous representation of the jet flow and sound fields is provided in Fig. 1, where an isosurface of q criterion colored by the jet velocity is represented inside the jet flow, and the pressure fluctuations $p' = p - p_\infty$ are represented outside. In the near-pressure field, straight, inclined acoustic waves are present near the jet and propagate with an angle of approximately 45 deg with respect to the flow direction. They are Mach waves produced by the supersonic motion of large-scale coherent structures inside the jet flow. At certain locations, as at $(r, z) = (-3r_0, 7r_0)$, for instance, the pressure levels due to these Mach waves are particularly high and the edges of the wave fronts display steep variations suggesting the presence of shocks.

The axial variations of the pressure levels on the surface defined in Sec. II.C are represented in Fig. 2a. The levels are low near the nozzle for $0 \leq z \leq 5r_0$ due to the fact that the mixing layers of the jet are not in a fully developed turbulent state close to the nozzle exit. Further downstream, the pressure levels rapidly increase and reach a peak of 3500 Pa at $z \simeq 8r_0$; after which, they gradually decrease with the axial distance. The skewness factors of the fluctuations of pressure and of dilatation $\Theta = \nabla \cdot \boldsymbol{u}$ are represented in Figs. 2b and 2c. For $z \geq 8r_0$, the skewness factors significantly deviate from the value of zero expected for Gaussian signals, indicating that the acoustic waves measured at these locations present a certain degree of nonlinearity consistent with the high-pressure levels. The positive skewness of the pressure implies that the maxima in the signals are stronger than the minima, whereas the negative skewness of the dilatation reveals the presence of steep compressions followed by gradual expansions. Such features are characteristic of the steepened waves observed in the pressure signals recorded in the near- [4,15] and far- [1,9] acoustic fields of jets emitting crackle noise.

The power spectrum density of the pressure fluctuations obtained at the location of peak levels, at $z = 8r_0$, is shown in Fig. 3a. It is broadband and centered around a peak Strouhal number $St = fD/u_j \simeq 0.6$, where f is the frequency. It also has a narrow shape similar to that of the acoustic spectra in the far fields of supersonic jets radiating Mach waves [3]. An example of the pressure signals recorded at the same location is shown in Fig. 3a. In this signal, two intense peaks, which are higher than three times the standard deviation, are visible at $t = 690r_0/a_\infty$. These peaks are preceded by a fast compression phase and followed by a gradual expansion, and are thus very similar to the shock-like structures observed in the far acoustic fields of supersonic jets [3,9]. Although the pressure levels at

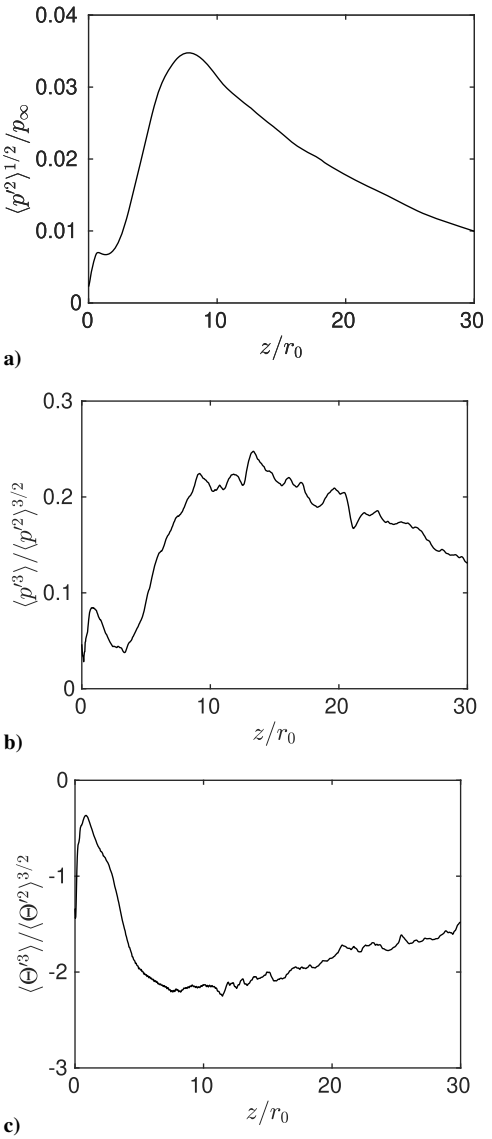

Fig. 2 Axial variations of the a) pressure levels, b) pressure skewness, and c) dilatation skewness on the conical surface.

this location are sufficiently high that the waveforms will steepen as they propagate due to nonlinear effects, the close proximity of the conical surface with the turbulent flow indicates that the distinctive, steepened shape of the waves is due, to a large extent, to the wave generation process. More particularly, the strong intermittency of the waves suggests that they are the result of intense intermittent events occurring inside the jet flow.

B. Conditional-Averaging Procedure

To identify and characterize the generation mechanisms of the steepened Mach waves close to the jets, a conditional-averaging procedure is applied. In this approach, extreme pressure peaks are extracted from the signals recorded on the conical surface and used in order to synchronize the flow and sound fields. Then, an ensemble average is performed so that the random, uncorrelated part of the signal is filtered out, revealing the coherent features of the flow correlated with the trigger peaks. This approach has been recently applied by the authors to describe the generation of steepened Mach waves near temporally developing jets [28–30,33]. Moreover, similar approaches have also been used to study noise generation mechanisms [47,48] and to identify and classify coherent structures in high-speed jets [49–51].

The pressure peaks are extracted by splitting the signals recorded at a given position in intervals of constant length τ. For each interval,

Downloaded by ECOLE CENTRAL DE LYON on May 8, 2021 | http://arc.aiaa.org | DOI: 10.2514/1.J059859

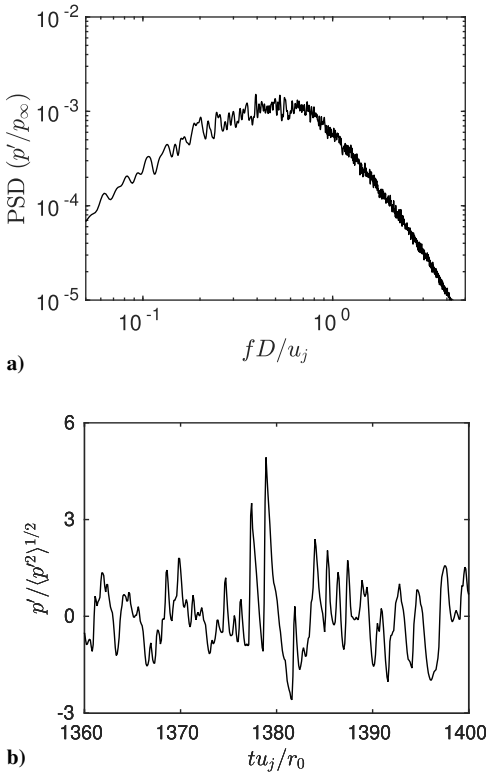

Fig. 3 Representation at $z = 8r_0$ and $r = 2.8r_0$ of the a) power spectrum density normalized by p_∞ and b) time variations of the pressure fluctuations.

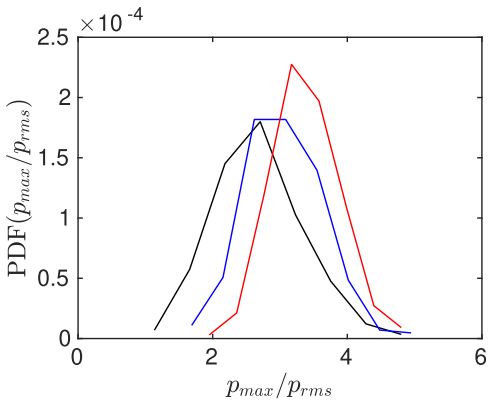

Fig. 4 PDF of the pressure peaks at $z = 8r_0$ and $r = 2.8r_0$ for interval length τ of $0.5r_0/a_\infty$ (black line), r_0/a_∞ (blue line), and $2r_0/a_\infty$ (red line).

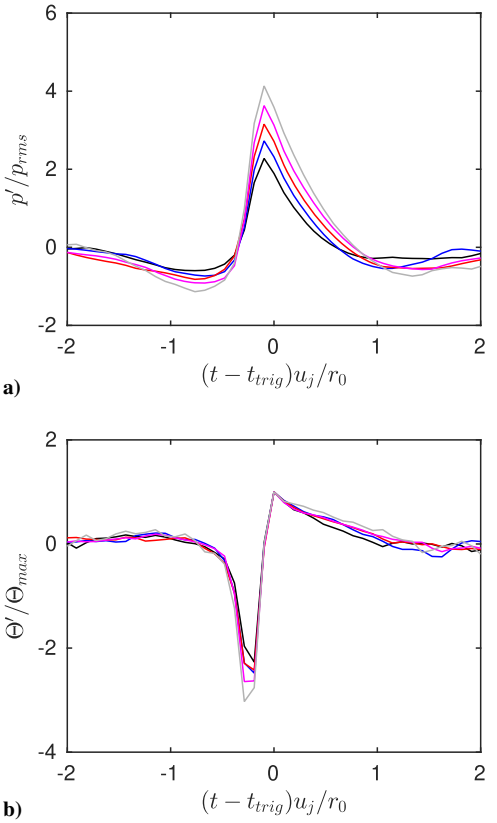

Fig. 5 Time variations of conditional a) pressure and b) dilatation at $z_{trig} = 8r_0$ and $r_{trig} = 2.8r_0$ for $p_{max} < 2.5p_{rms}$ (black line), $2.5p_{rms} \le p_{max} < 3p_{rms}$ (blue line), $3p_{rms} \le p_{max} < 3.5p_{rms}$ (red line), $3.5p_{rms} \le p_{max} < 4p_{rms}$ (magenta line), and $p_{max} \ge 4p_{rms}$ (gray line).

the maximum of the pressure fluctuations is determined over the entire circumference of the jet and their times t_{trig} and azimuthal positions θ_{trig} are stored. The normalized probability density functions (PDFs) of the pressure peaks at $z_{trig} = 8r_0$ and $r_{trig} = 2.75r_0$, at the location of peak levels, are shown in Fig. 4 for different values of the interval length τ ranging from $0.5r_0/a_\infty$ to $2r_0/a_\infty$. The distributions are not symmetric about their peak, as expected for the PDF of the maxima of random variables. When τ is increased, the maximum of the PDF is shifted toward higher values so that the intervals have stronger peaks. For instance, 28, 50, and 78% of the pressure peaks are higher than $3p_{rms}$ for $T = 0.5r_0/a_\infty$, r_0/a_∞, and $2r_0/a_\infty$, respectively. Since one objective of the present study is to compare the flow structures correlated with moderate and high-intensity pressure peaks, the value $\tau = r_0/a_\infty$ is used in what follows because it allows us to extract a wide spectrum of peak amplitudes, ranging from values lower than $2.5p_{rms}$ to values higher than $4p_{rms}$. Moreover, this time scale corresponds to a Strouhal number of one, which is close to the peak of the spectra in Fig. 3a. The detection procedure is performed at 10 different trigger positions z_{trig} evenly distributed every r_0 on the conical surface, ranging from $z = 6r_0$, where the pressure skewness becomes significant in Fig. 2a, down to the end of the potential core at $z = 15r_0$.

Before computing the averages, the extracted peaks are distributed into five groups according to their magnitudes. The first group contains the peaks whose amplitude p_{max} is lower than $2.5p_{rms}$, whereas the others contain the peaks such that $2.5p_{rms} \le p_{max} < 3p_{rms}$, $3p_{rms} \le p_{max} < 3.5p_{rms}$, $3.5p_{rms} \le p_{max} < 4p_{rms}$, and $4p_{rms} \ge p_{max}$. For $z_{trig} = 8r_0$, for instance, at the location of peak pressure levels, these groups contain 136, 266, 232, 127, and 40 events, respectively. The conditionally averaged pressure signals at this location are plotted in Fig. 5a. The signals obtained for the five groups are very similar and consist of a fast compression phase for $t \le t_{trig}$ followed by a gradual expansion phase for $t > t_{trig}$. Thus, they possess the main features of the steepened waves associated with crackle. It can also be noted that the present structures are very similar to the ones extracted by Baars and Tinney [3], who applied a shock detection algorithm to pressure signals recorded in the far acoustic field of a cold Mach 3 jet. Since the present analysis is performed in the very near vicinity of the jet flow, this suggests that the distinctive, steepened shapes of the structures already exist at the time when they are generated inside the turbulent flow.

The conditional dilatation signals are represented in Fig. 5a. They are normalized by their maxima in order to illustrate how the shapes of the waveforms vary with the magnitude of the trigger pressure peaks. In these signals, a marked negative spike due to the steep compression phase is followed by a wide low-amplitude positive peak related to the expansion phase. The ratio between the minimum and the maximum dilatations increases with the magnitude of the pressure peak, in absolute value. This shows that the slope of the compression phase is more pronounced with respect to that of the expansion phase when the wave amplitude is higher, suggesting a stronger nonlinear behavior.

Downloaded by ECOLE CENTRAL DE LYON on May 8, 2021 | http://arc.aiaa.org | DOI: 10.2514/1.J059859

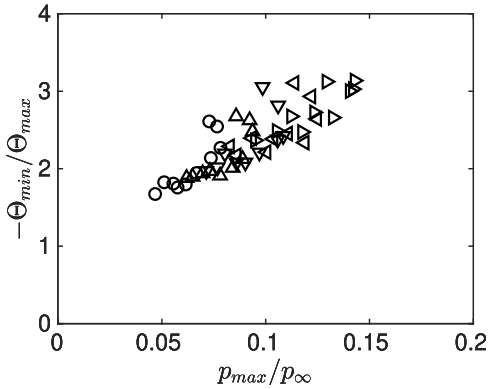

Fig. 6 Conditional steepening factor as a function of the conditional pressure peak for $6r_0 \le z_{trig} \le 15r_0$ and $p_{max} < 2.5p_{rms}$ (circles), $2.5p_{rms} \le p_{max} < 3p_{rms}$ (triangles), $3p_{rms} \le p_{max} < 3.5p_{rms}$ (bottom-facing triangles), $3.5p_{rms} \le p_{max} < 4p_{rms}$ (left-facing triangles), and $p_{max} \ge 4p_{rms}$ (right-facing triangles).

A conditional steepening factor (CSF) defined as $\mathrm{CSF} = -\Theta_{min}/\Theta_{max}$ is introduced, where Θ_{min} and Θ_{max} are the minimum and maximum values of the conditional dilatation. It can be viewed as a conditional version of the wave-steepening factor introduced by Gallagher and McLaughlin [8], which was used in Refs. [3,9] to assess the nonlinearity of the acoustic waves radiated by supersonic jets. The CSF measures the degree of asymmetry between the compression and expansion phases in a given waveform. While $\mathrm{CSF} = 1$ corresponds to the case of a smooth, harmonic wave, values higher than one indicate steepened waves. The conditional steepening factor computed on the conical surface for $6r_0 \le z_{trig} \le 15r_0$, at the locations indicated as black circles in Fig. 1, and for the five sets of pressure peaks is plotted in Fig. 6 as a function of the conditional pressure peak. It seems to increase linearly so that the highest conditional steepening factors can be associated with the most intense pressure peaks. It can also be noted that all of the CSF values are significantly higher than one, indicating that steepened waves are detected for all of the axial positions considered, which span a large extent of the developing jet shear layer.

C. Coherent Structures Correlated with the Steepened Waves

The conditional-averaging procedure is now used to describe the flow events correlated with the steepened Mach waves with the aim to identify their generation mechanisms. For that, the fields are synchronized with respect to the time t_{trig} and the azimuthal coordinate θ_{trig} of the pressure peaks, and then they are averaged. Due to the prohibitive memory cost of storing thousands of three-dimensional arrays of data, the flow and sound fields of the jet are reconstructed using their first five azimuthal Fourier modes before the ensemble-average operation. This is justified based on the observation in Ref. [28] that using the first five azimuthal modes is sufficient to recover the main features of the steepened waves radiated by the shear layers of supersonic jets.

The conditional fields of vorticity and pressure fluctuations obtained for $z_{trig} = 8r_0$ are represented in Fig. 7 at six times between $t_{trig} - 4r_0/a_\infty$ and $t_{trig} + 6r_0/a_\infty$. In this figure, the conditional fields are obtained using all pressure peaks so that a total of 801 events are used. The mean vorticity is subtracted in order to remove the component due to the mean shear. The structure of the jet is also represented by showing isocontours of the conditional axial velocity for the values of $u_z = 0.95u_j$, a_∞, and $0.05u_j$, which represent the limit of the potential core, the sonic line, and the outer edge of the jet, respectively. In the pressure field, the conditional waveform possesses a distinctive wave-packet structure with an inclination angle of approximately 45 deg with respect to the jet direction. It is attached to the jet flow at times preceding the trigger t_{trig} and propagates away for $t > t_{trig}$. Inside the jet, the wave is connected to a large-scale vorticity excess located beneath the sonic line and surrounded by two small spots of vorticity deficit. This flow pattern is convected downstream with the wave and can be interpreted as the footprint of the coherent structures in the shear layers. More particularly, the vorticity excess is the trace of large-scale vortices, whereas the vorticity deficits correspond to the stagnation points upstream and downstream of the vortex. When convected at a supersonic speed, these structures act upon the ambient medium in a way similar to that of a supersonic travelling wavy surface, leading to the generation of Mach waves. As argued by Buchta and Freund [27], the waves generated by such wavy-wall disturbances can steepen due to nonlinear gas dynamics effects when the intensity of the perturbation is strong enough or when their convection speeds are sufficiently high. In the remainder of the paper, the relationship between the intensity of the trigger pressure peaks and properties of the coherent structures, including their convection speed, strength, and geometrical shape, are investigated.

1. Convection Speed

The convection speeds of the coherent structures are estimated from the conditional-averaged fields by tracking the location of peak vorticity as a function of time and by performing a linear regression. This estimation is carried out separately for the five groups of events in order to identify a possible link between the intensity of the peaks and the convection velocity of the structures. The convection speeds for the five groups are represented in Fig. 8 as a function of the trigger position z_{trig}. For all groups of events, and for all of the locations considered, it is between $0.7u_j$ and $0.8u_j$, which is in good agreement with the values found in the literature for jets at similar exhaust conditions [19]. It is also significantly higher than the ambient sound speed, and it is consistent with the propagation angle of 45 deg, according to Eq. (1). The convection speed estimated from the conditional averages triggered by the most intense pressure peaks does not appreciably differ from that triggered from the less intense ones. Thus, there is no clear link between the magnitude of the pressure peaks and the convection speed of the coherent structures in the present jet.

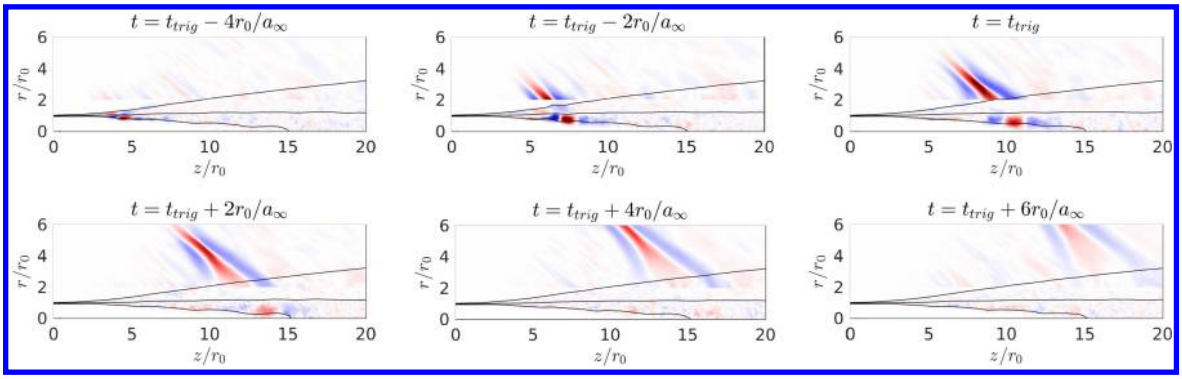

Fig. 7 Representation of conditional pressure fluctuations outside the jet and of conditional vorticity norm inside. Scales range within ±5000 Pa for pressure and $\pm u_j/r_0$ for vorticity. Solid lines indicate contours of conditional axial velocity for values $0.95u_j$, $a_\infty = 0.5u_j$, and $0.05u_j$.

Downloaded by ECOLE CENTRAL DE LYON on May 8, 2021 | http://arc.aiaa.org | DOI: 10.2514/1.J059859

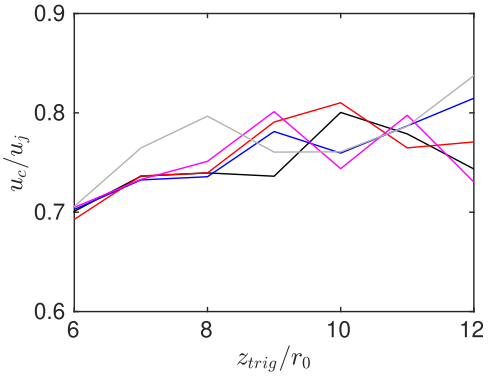

Fig. 8 Axial variations of the convection speed for $p_{max} < 2.5p_{rms}$ (black line), $2.5p_{rms} \le p_{max} < 3p_{rms}$ (blue line), $3p_{rms} \le p_{max} < 3.5p_{rms}$ (red line), $3.5p_{rms} \le p_{max} < 4p_{rms}$ (magenta line), and $p_{max} \ge 4p_{rms}$ (gray line).

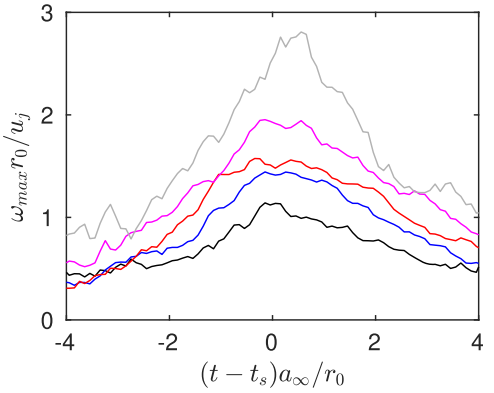

Fig. 9 Maximum conditional vorticity for $z_{trig} = 8r_0$ as a function of $t - t_s$, where $t_s = t_{trig} - r_{trig}/a_\infty$ for $p_{max} < 2.5p_{rms}$ (black line), $2.5p_{rms} \le p_{max} < 3p_{rms}$ (blue line), $3p_{rms} \le p_{max} < 3.5p_{rms}$ (red line), $3.5p_{rms} \le p_{max} < 4p_{rms}$ (magenta line), and $p_{max} \ge 4p_{rms}$ (gray line).

2. *Strength of the Coherent Structures*

The mean strength of the coherent structures correlated with the steepened waves is characterized, following Zaman and Hussain [49], by considering the maximum of conditional vorticity. The time variations of this maximum are plotted in Fig. 9 for the trigger position $z_{trig} = 8r_0$ for the five groups of events. In all cases, the maximum vorticity grows and reaches a peak at $t_s = t_{trig} - r_{trig}/a_\infty$, and it rapidly decreases afterward as the structure decays and vanishes. Moreover, the vorticity level is higher for stronger trigger peaks, indicating that the intensity of the waves increases with the strength of the coherent structures. To confirm this, the maximum vorticity at $t = t_s$ is plotted in Fig. 10a as a function of the pressure peak for different trigger positions z_{trig}. represented as black circles in Fig. 1 for the five groups of events. An approximately linear relationship is obtained, which illustrates that Mach wave radiation is essentially a linear phenomenon. The nonlinear behavior of the waves, represented by the conditional steepening factor in Fig. 10a, also increases with the strength of the vortical structures. Therefore, the strongest large-scale vortices are those that generate the most intense but also the steepest acoustic waves.

3. *Geometrical Shape of the Coherent Structures*

Finally, the link between the steepened Mach waves and the geometrical shape of the coherent structures that generate them is explored. For that, the conditional fields of vorticity for $z_{trig} = 8r_0$ are represented in Fig. 11 at $t_s = t_{trig} - r_{trig}/a_\infty$ for three of the five groups of events. The first group contains the weakest events such that $p_{max} < 2.5p_{rms}$; the second one contains the events of medium intensity, for which $2.5p_{rms} \le p_{max} < 3.5p_{rms}$; and the third group contains the strongest events such that $p_{max} \ge 4p_{rms}$. The conditional

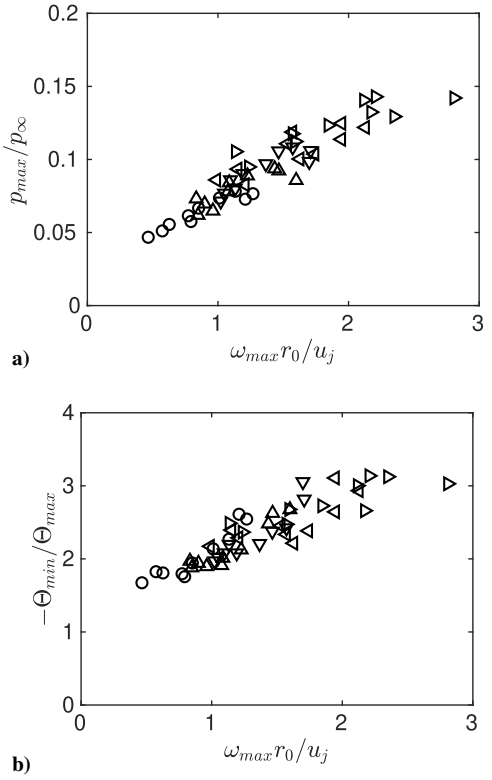

Fig. 10 Maximum conditional a) pressure and b) steepening factor as a function of the peak conditional vorticity for $p_{max} < 2.5p_{rms}$ (circles), $2.5p_{rms} \le p_{max} < 3p_{rms}$ (triangles), $3p_{rms} \le p_{max} < 3.5p_{rms}$ (bottom-facing triangles), $3.5p_{rms} \le p_{max} < 4p_{rms}$ (left-facing triangles), and $p_{max} \ge 4p_{rms}$ (right-facing triangles).

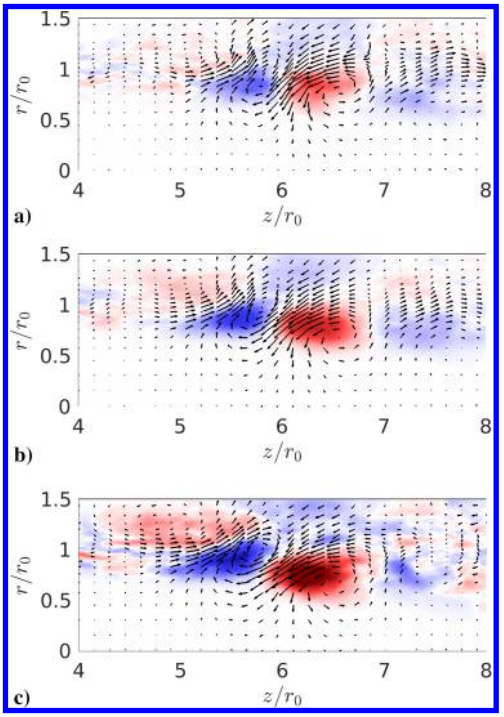

Fig. 11 Representation at $t = t_s$ of the conditional velocity as a vector field with the vorticity in color scale for a) $p_{max} < 2.5p_{rms}$, b) $3p_{rms} < p_{max} \le 3.5p_{rms}$, and c) $p_{max} \ge 4p_{rms}$. The scale for the vorticity ranges within $\pm 2u_j/r_0$.

velocity field is also represented as a vector field in order to visualize the trace of the coherent structures. The fields in the three cases share the same general features, namely, a vorticity excess associated with a

Downloaded by ECOLE CENTRAL DE LYON on May 8, 2021 | http://arc.aiaa.org | DOI: 10.2514/1.J059859

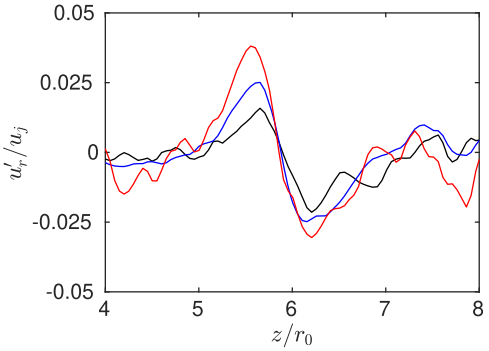

Fig. 12 Profiles of conditional radial velocity fluctuations at $t = t_s$ and $r = 1.2r_0$ for $p_{max} < 2.5p_{rms}$ (black line), $3p_{rms} \leq p_{max} < 3.5p_{rms}$ (blue line), and $p_{max} \geq 4p_{rms}$ (red line).

large-scale vortex and followed by a vorticity deficit corresponding to the stagnation point downstream from the vortex. The shape of the structures depends on the magnitude of the trigger pressure peak. For the weakest group of events, in Fig. 11a, the vortex and its stagnation point are aligned with respect to the flow direction. However, for the medium-intensity events in Fig. 11b and (to a larger extent) for the strongest events in Fig. 11c, the center of the vortex is located deeper inside the jet flow than the stagnation point, so that the flow disturbance is slightly inclined towards the jet axis with respect to the flow direction. This effect is also visible in the profiles of conditional radial velocity just above the vortex structure at $r = 1.2r_0$, represented in Fig. 12. For all groups of events, the profiles consist of a peak followed by a trough. The amplitude of the peak is very close to that of the trough for the weakest group of events due to the fact that the vortex center and stagnation point are aligned in the flow direction. For the medium- and high-intensity events, however, the peak is significantly higher than the trough in absolute value. This asymmetry of the profile can help us explain, at least qualitatively, why the inclined structures generate stronger acoustic waves than the others. Indeed, coherent structures in high-speed jets generate sound by a mechanism analogous to that of a wavy surface convected at a supersonic speed. This wavy-wall analogy can help us provide a simplified model of the sound generation mechanisms at play by considering a two-dimensional wall profile based on the variations of the conditional radial velocity in Fig. 12. In a frame of reference moving with the structure at a supersonic convection speed, positive radial velocities, corresponding to positive slopes of the wall, will lead to overpressures while negative velocities will be associated with underpressures. As a consequence, the asymmetric profile obtained for the strongest group of events is likely to generate pressure waveforms with peaks stronger than troughs, thus promoting (for a given amplitude of the perturbation) the formation of intense, positively skewed acoustic waves. Despite the coherent structures depicted earlier in this paper being significantly more complex than a simple wavy wall and that the choice of considering the velocity profile at $r = 1.2r_0$ is arbitrary, this provides a simple explanation of the mechanisms by which the geometrical shape of the coherent structures can influence the strength and asymmetry of the Mach waves they generate.

IV. Conclusions

In the present study, the generation of steepened Mach waves in the near-acoustic field of an isothermal Mach 2 jet is investigated by examining a numerical simulation database obtained using the large-eddy simulation. The pressure fluctuations recorded on a conical surface located in the near vicinity of the flow and spreading with the jet are found to display intense acoustic waves with rapid compressions and gradual expansions. The presence of these waves so close from the turbulent flow indicates that their steepened aspect is due, to a large extent, to nonlinear mechanisms occurring inside the jet. Besides, their strong directivities and large wavelengths suggest that they are a particular, nonlinear case of Mach waves. It is first shown that the steepened aspect of the waves is directly linked to their amplitude, which confirms the nonlinearity of the steepening mechanisms involved. Then, the wave-steepening process is investigated by performing conditional averages triggered by the detection of intense pressure peaks at different axial locations on the conical surface. These averages allow us to establish a direct link between the generation of steepened Mach waves and the supersonic convection of large-scale coherent structures located in the high-speed supersonic core of the jet. The averages are computed separately for different groups of events corresponding to different magnitudes of the trigger pressure peaks. It is first found that the strongest and weakest waves are generated by coherent structures travelling at very similar speeds. Thus, the wide range of wave amplitudes and steepening factors measured near the jet is not due to variations of the convection speed. The strength of the structures, however, plays an important role because the peak of conditional pressure is linearly related to the maximum of conditional vorticity. As a result, the most intense acoustic waves are generated by the strongest coherent structures, which are also those that generate the steepest waves. Finally, the structures correlated with the strongest trigger peaks are more inclined than the others with respect to the flow direction. Following the wavy-wall analogy, the asymmetric shape of these structures causes the generation of positively skewed Mach waves, which favors their steepening through nonlinear effects. Therefore, it appears that the strength and geometrical shapes of the structures are the most important characteristics pertaining to the generation of steepened Mach waves. These results could help us investigate how noise reduction devices such as chevrons, nozzle inserts, or microjets act upon the properties of coherent structures, which could be useful in order to optimize noise mitigation strategies.

Acknowledgments

This work was granted access to the High Performance Computing resources of Pôle de Modélisation et de Calcul en Sciences de l'Ingénieur et de l'Information (PMCS2I) of Ecole Centrale de Lyon, Pôle Scientifique de Modélisation Numérique (PSMN) of École Normale Supérieure (ENS) de Lyon and Pôle de Calcul Hautes Performances Dédiés (P2CHPD) of Université Lyon I, members of Fédération Lyonnaise de Modélisation et Sciences Numériques (FLMSN), partner of Equipement d'excellence (EQUIPEX) EQUIP@MESO, and to the resources of Institut du Développement et des Ressources en Informatique Scientifique (IDRIS) under the allocation 2019-2a0204 made by Grand Equipement National de Calcul Intensif (GENCI). It was performed within the framework of the Laboratoire d'Excellence Centre Lyonnais d'Acoustique (LABEX CeLyA) (ANR-10-LABX-0060) of Université de Lyon, within the program Investissements d'Avenir (ANR-16-IDEX-0005) operated by the French National Research Agency (ANR).

References

[1] Ffowcs Williams, J. E., Simson, J., and Virchis, V. J., "'Crackle': An Annoying Component of Jet Noise," *Journal of Fluid Mechanics*, Vol. 71, No. 2, 1975, pp. 251–271. https://doi.org/10.1017/S0022112075002558

[2] Laufer, J., Schlinker, R., and Kaplan, R. E., "Experiments on Supersonic Jet Noise," *AIAA Journal*, Vol. 14, No. 4, 1976, pp. 489–497. https://doi.org/10.2514/3.61388

[3] Baars, W. J., and Tinney, C. E., "Shock-Structures in the Acoustic Field of a Mach 3 Jet with Crackle," *Journal of Sound and Vibration*, Vol. 333, No. 12, 2014, pp. 2539–2553. https://doi.org/10.1016/j.jsv.2014.01.008

[4] Mora, P., Heeb, N., Kastner, J., Gutmark, E. J., and Kailasanath, K., "Impact of Heat on the Pressure Skewness and Kurtosis in Supersonic Jets," *AIAA Journal*, Vol. 52, No. 4, 2014, pp. 777–787. https://doi.org/10.2514/1.J052612

[5] Krothapalli, A., Venkatakrishnan, L., and Lourenco, L., "Crackle: A Dominant Component of Supersonic Jet Mixing Noise," AIAA Paper 2000-2024, 2000. https://doi.org/10.2514/6.2000-2024

[6] Schlinker, R., Liljenberg, S., Polak, D., Post, K., and Chipman, C., "Supersonic Jet Noise Source Characteristics and Propagation: Engine and Model Scale," AIAA Paper 2007-3623, 2007. https://doi.org/10.2514/6.2007-3623

Downloaded by ECOLE CENTRAL DE LYON on May 8, 2021 | http://arc.aiaa.org | DOI: 10.2514/1.J059859

[7] Gee, K. L., Sparrow, V. W., James, M. M., Downing, J. M., Hobbs, C. M., Gabrielson, T. B., and Atchley, A. A., "The Role of Nonlinear Effects in the Propagation of Noise from High-Power Jet Aircraft," *Journal of the Acoustical Society of America*, Vol. 123, No. 6, 2008, pp. 4082–4093. https://doi.org/10.1121/1.2903871

[8] Gallagher, J., and McLaughlin, D., "Experiments on the Nonlinear Characteristics of Noise Propagation from Low and Moderate Reynolds Number Supersonic Jets," AIAA Paper 1981-2041, 1981. https://doi.org/10.2514/6.1981-2041

[9] Fiévet, R., Tinney, C. E., Baars, W. J., and Hamilton, M. F., "Coalescence in the Sound Field of a Laboratory-Scale Supersonic Jet," *AIAA Journal*, Vol. 54, No. 1, 2016, pp. 254–265. https://doi.org/10.2514/1.J054252

[10] Lighthill, J., "The Inaugural Theodorsen Lecture: Some Aspects of the Aeroacoustics of High-Speed Jets," *Theoretical and Computational Fluid Dynamics*, Vol. 6, No. 5, 1994, pp. 261–280. https://doi.org/10.1007/BF00311841

[11] Gurbatov, S. N., and Rudenko, O. V., "Statistical Phenomena", *Nonlinear Acoustics*, edited by M. F. Hamilton, and D. T. Blackstock, Academic Press, San Diego, CA, 1998, pp. 377–398, Chap. 13.

[12] Baars, W., Tinney, C. E., Wochner, M. S., and Hamilton, M. F., "On Cumulative Nonlinear Acoustic Waveform Distorsions from High-Speed Jets," *Journal of Fluid Mechanics*, Vol. 749, June 2014, pp. 331–366. https://doi.org/10.1017/jfm.2014.228

[13] Papamoschou, D., "Evidence of Shocklets in a Counterflow Supersonic Shear Layer," *Physics of Fluids*, Vol. 7, No. 2, 1995, pp. 233–235. https://doi.org/10.1063/1.868621

[14] Rossmann, T., Mungal, M. G., and Hanson, R. K., "Evolution and Growth of Large-Scale Structures in High Compressibility Mixing Layers," *Journal of Turbulence*, Vol. 3, 2002, Paper N9. https://doi.org/10.1088/1468-5248/3/1/009

[15] Nichols, J. W., Lele, S. K., Ham, F. E., Martens, S., and Spyropoulos, J. T., "Crackle Noise in Heated Supersonic Jets," *Journal of Engineering for Gas Turbines and Power*, Vol. 135, No. 5, 2013, Paper 051202. https://doi.org/10.1115/1.4007867

[16] Buchta, D. A., and Freund, J. B., "The Near-Field Pressure Radiated by Planar High-Speed Free-Shear-Flow Turbulence," *Journal of Fluid Mechanics*, Vol. 832, Dec. 2017, pp. 383–408. https://doi.org/10.1017/jfm.2017.671

[17] Freund, J. B., Lele, S. K., and Moin, P., "Numerical Simulation of a Mach 1.92 Turbulent Jet and its Sound Field," *AIAA Journal*, Vol. 38, No. 11, 2000, pp. 2023–2031. https://doi.org/10.2514/2.889

[18] Tam, C. K. W., "Supersonic Jet Noise," *Annual Review of Fluid Mechanics*, Vol. 27, No. 1, 1995, pp. 17–43. https://doi.org/10.1146/annurev.fl.27.010195.000313

[19] Troutt, T. R., and McLaughlin, D. K., "Experiments on the Flow and Acoustic Properties of a Moderate-Reynolds-Number Supersonic Jet," *Journal of Fluid Mechanics*, Vol. 116, March 1982, pp. 123–156. https://doi.org/10.1017/S0022112082000408

[20] Tam, C. K. W., and Burton, D. E., "Sound Generated by Instability Waves of Supersonic Flows. Part 1. Two-Dimensional Mixing Layers," *Journal of Fluid Mechanics*, Vol. 138, Jan. 1984, pp. 249–271. https://doi.org/10.1017/S0022112084000112

[21] Tam, C. K. W., and Burton, D. E., "Sound Generated by Instability Waves of Supersonic Flows. Part 2. Axisymmetric Jets," *Journal of Fluid Mechanics*, Vol. 138, Jan. 1984, pp. 273–295. https://doi.org/10.1017/S0022112084000124

[22] Tam, C. K. W., and Chen, P., "Turbulent Mixing Noise from Supersonic Jets," *AIAA Journal*, Vol. 32, No. 9, 1994, pp. 1774–1780. https://doi.org/10.2514/3.12173

[23] Sinha, A., Rodriguez, D., Brès, G. A., and Colonius, T., "Wavepacket Models for Supersonic Jet Noise," *Journal of Fluid Mechanics*, Vol. 742, March 2014, pp. 71–95. https://doi.org/10.1017/jfm.2013.660

[24] Martens, S., Spyropoulos, J. T., and Nagel, Z., "The Effects of Chevrons on Crackle-Engine and Scale Model Results," *Proceedings of the ASME Turbo Expo*, American Soc. of Mechanical Engineers Paper GT2011-46417, New York, 2011.

[25] Krothapalli, A., Greska, B., and Arakeri, V., "High Speed Jet Noise Reduction Using Microjets," AIAA Paper 2002-2450, 2002. https://doi.org/10.2514/6.2002-2450

[26] Murray, N. E., and Lyons, G. W., "On the Convection Velocity of Source Events Related to Supersonic Jet Crackle," *Journal of Fluid Mechanics*, Vol. 793, April 2016, pp. 477–503. https://doi.org/10.1017/jfm.2016.127

[27] Buchta, D. A., and Freund, J. B., "Intense Sound Radiation by High-Speed Flow: Turbulence Structure, Gas Properties, and Near-Field Gas Dynamics," *Physical Review Fluids*, Vol. 4, No. 4, 2019, Paper 044605. https://doi.org/10.1103/PhysRevFluids.4.044605

[28] Pineau, P., and Bogey, C., "Steepened Mach Waves near Supersonic Jets: Study of Azimuthal Structure and Generation Process Using Conditional Averages," *Journal of Fluid Mechanics*, Vol. 880, Dec. 2019, pp. 594–619. https://doi.org/10.1017/jfm.2019.729

[29] Bogey, C., and Pineau, P., "Potential-Core Closing of Temporally Developing Jets at Mach Numbers Between 0.3 and 2: Scaling and Conditional Averaging of Flow and Sound Fields," *Physical Review Fluids*, Vol. 4, No. 12, 2019, Paper 124601. https://doi.org/10.1103/PhysRevFluids.4.124601

[30] Pineau, P., and Bogey, C., "Temperature Effects on Convection Speed and Steepened Waves of Temporally Developing Supersonic Jets," *AIAA Journal*, Vol. 58, No. 3, 2020, pp. 1227–1239. https://doi.org/10.2514/1.J058589

[31] Dimotakis, P. E., "Two Dimensional Shear-Layer Entrainment," *AIAA Journal*, Vol. 24, No. 11, 1986, pp. 1791–1796. https://doi.org/10.2514/3.9525

[32] Brown, G. L., "The Entrainment and Large Structures in Turbulent Mixing Layers," *Proceeding of the 5th Autralasian Conference on Hydraulics and Fluid Mechanics*, Univ. of Canterbury, 1974, pp. 352–359.

[33] Bogey, C., "On Noise Generation in Low Reynolds Number Temporal Round Jets at a Mach Number of 0.9," *Journal of Fluid Mechanics*, Vol. 859, Jan. 2019, pp. 1022–1056. https://doi.org/10.1017/jfm.2018.864

[34] Avital, E. J., Musafir, R. E., and Korakianitis, T., "Nonlinear Propagation of Sound Emitted by High Speed Wave Packets," *Journal of Computational Acoustics*, Vol. 21, No. 2, 2013, Paper 250027. https://doi.org/10.1142/S0218396X12500270

[35] Zaman, K. B. M. Q., "Effect of Initial Condition on Subsonic Jet Noise," *AIAA Journal*, Vol. 23, No. 9, 1985, pp. 1370–1373. https://doi.org/10.2514/3.9094

[36] Bogey, C., Bailly, C., and Marsden, O., "Large Eddy Simulation of the Flow and Acoustic Field of a Reynolds Number Subsonic Jet with Tripped Exit Boundary Layers," *Physics of Fluids*, Vol. 23, No. 3, 2011, Paper 035104. https://doi.org/10.1063/1.3555634

[37] Gojon, R., and Bogey, C., "Numerical Study of the Flow and the near Acoustic Fields of an Underexpanded Round Free Jet Generating Two Screech Tones," *International Journal of Aeroacoustics*, Vol. 16, Nos. 7–8, 2017, pp. 603–625. https://doi.org/10.1177/2F1475472X17727606

[38] Nonomura, T., Nakano, H., Ozawa, Y., Terakado, D., Yamamoto, M., Fujii, K., and Oyama, A., "Large Eddy Simulation of Acoustic Waves Generated from a Hot Supersonic Jet," *Shock Waves*, Vol. 29, No. 8, 2019, pp. 1133–1154. https://doi.org/10.1007/s00193-019-00895-2

[39] Bogey, C., and Bailly, C., "A Family of Low Dispersive and Low Dissipative Explicit Schemes for Noise Computation," *Journal of Computational Physics*, Vol. 194, No. 1, 2004, pp. 194–214. https://doi.org/10.1016/j.jcp.2003.09.003

[40] Bogey, C., and Bailly, C., "Computation of a High Reynolds Number Jet and Its Radiated Noise Using Large-Eddy Simulation Based on Explicit Filtering," *Computers and Fluids*, Vol. 35, No. 10, 2006, pp. 1344–1358. https://doi.org/10.1016/j.compfluid.2005.04.008

[41] Bogey, C., and Bailly, C., "Turbulence and Energy Budget in a Self-Preserving Round Jet: Direct Evaluation Using Large Eddy Simulation," *Journal of Fluid Mechanics*, Vol. 627, May 2009, pp. 129–160. https://doi.org/10.1017/S0022112009005801

[42] Bogey, C., de Cacqueray, N., and Bailly, C., "A Shock-Capturing Methodology Based on Adaptative Spatial Filtering for High-Order Non-Linear Computations," *Journal of Computational Physics*, Vol. 228, No. 5, 2009, pp. 1447–1465. https://doi.org/10.1016/j.jcp.2008.10.042

[43] Mohseni, K., and Colonius, T., "Numerical Treatment of Polar Coordinate Singularities," *Journal of Computational Physics*, Vol. 157, No. 10, 2002, pp. 3593–3600. https://doi.org/10.1006/jcph.1999.6382

[44] Bogey, C., de Cacqueray, N., and Bailly, C., "Finite Differences for Coarse Azimuthal Discretization and for Reduction of Effective Resolution Near Origin of Cylindrical Flow Equations," *Journal of Computational Physics*, Vol. 230, No. 4, 2011, pp. 1134–1146. https://doi.org/10.1016/j.jcp.2010.10.031

[45] Tam, C. K. W., and Dong, Z., "Radiation and Outflow Boundary Conditions for Direct Computation of Acoustic and Flow Disturbances in a Nonuniform Mean Flow," *Journal of Computational Acoustics*, Vol. 4, No. 2, 1996, pp. 175–201. https://doi.org/10.1142/S0218396X96000040

Downloaded by ECOLE CENTRAL DE LYON on May 8, 2021 | http://arc.aiaa.org | DOI: 10.2514/1.J059859

[46] Bogey, C., and Bailly, C., "Three-Dimensional Non-Reflective Boundary Conditions for Acoustic Simulations: Far Field Formulation and Validation Test Cases," *Acta Acustica United with Acustica*, Vol. 88, No. 4, 2002, pp. 463–471.

[47] Arroyo, C. P., Daviller, G., Puigt, G., Airiau, C., and Moreau, S., "Identification of Temporal and Spatial Signatures of Broadband Shock-Associated Noise," *Shock Waves*, Vol. 29, No. 1, 2019, pp. 117–134. https://doi.org/10.1007/s00193-018-0806-4

[48] Schmidt, O. T., and Schmid, P. J., "A Conditional Space-Time POD Formalism for Intermittent and Rare Events: Example of Acoustic Bursts in Turbulent Jets," *Journal of Fluid Mechanics*, Vol. 867, May 2019, Paper R2. https://doi.org/10.1017/jfm.2019.200

[49] Zaman, K. B. M. Q., and Hussain, A. K. M. F., "Natural Large-Scale Structures in the Axisymmetric Mixing Layer," *Journal of Fluid Mechanics*, Vol. 138, Jan. 1984, pp. 325–351. https://doi.org/10.1017/S0022112084000148

[50] Lau, J. C., and Fisher, M. J., "The Vortex-Street Structure of 'Turbulent' Jets. Part 1," *Journal of Fluid Mechanics*, Vol. 67, No. 2, 1975, pp. 299–337. https://doi.org/10.1017/S0022112075000328

[51] Mayo, D. E., Daniel, K., Lowe, T., and Ng, W., "Statistical Flow Structures in Heated Supersonic Jets with Offset Temperature Non-Uniformities," AIAA Paper 2019-2708, 2019. https://doi.org/10.2514/6.2019-2708

D. Papamoschou
Associate Editor

Downloaded by ECOLE CENTRAL DE LYON on May 8, 2021 | http://arc.aiaa.org | DOI: 10.2514/1.J059859